

Band crossover and magnetic phase diagram of high- T_C superconducting compound $\text{Ba}_2\text{CuO}_{4-\delta}$

Xiao-Cheng Bai^{1,2,*}, Ya-Min Quan^{1,*}, H.-Q. Lin^{3,4}, and Liang-Jian Zou^{1,2†}

¹ Key Laboratory of Materials Physics,
Institute of Solid State Physics, HFIPS,

Chinese Academy of Sciences, Hefei 230031, China

² Science Island Branch of Graduate School,

University of Science and Technology of China, Hefei 230026, China

³ Beijing Computational Science Research Center,
Beijing 100193, China

⁴ Department of Physics,

Beijing Normal University, Beijing 100875, China

(Dated: today)

We present the influences of electronic and magnetic correlations and doping evolution on the groundstate properties of recently discovered superconductor $\text{Ba}_2\text{CuO}_{4-\delta}$ by utilizing the Kotliar-Ruckenstein slave boson method. Starting with an effective two-orbital Hubbard model (Scalapino *et al.* Phys. Rev. **B 99**, 224515 (2019)), we demonstrate that with increasing doping concentration, the paramagnetic (PM) system evolves from two-band character to single-band ones around the electron filling $n=2.5$, with the band nature of the $d_{3z^2-y^2}$ and $d_{x^2-y^2}$ orbitals to the $d_{x^2-y^2}$ orbital, slightly affected when the electronic correlation U varies from 2 to 4 eV. Considering the magnetic correlations, the system displays one antiferromagnetically metallic (AFM) phase in $2 < n < 2.16$ and a PM phase in $n > 2.16$ at $U=2$ eV, or two AFM phases in $2 < n < 2.57$ and $2.76 < n < 3$, and a PM phase in $2.57 < n < 2.76$ respectively, at $U=4$ eV. Our results show that near realistic superconducting state around $n=2.6$ the intermediate correlated $\text{Ba}_2\text{CuO}_{3.2}$ should be single band character, and the s-wave superconducting pairing strength becomes significant when $U>2$ eV, and crosses over to d-wave when $U>2.2$ eV.

PACS numbers: 74.72.-h, 71.30.+h, 75.30.Kz, 71.27.+a

I. INTRODUCTION

The discovery of newly cuprate superconductor $\text{Ba}_2\text{CuO}_{4-\delta}$ with high T_c of 70 K^1 , about 2 to 3 times higher than isostructural conventional cuprate $\text{La}_2\text{CuO}_{4-\delta}$, have stirred great interesting on its essential electronic states and superconducting properties²⁻⁹. Though being isostructural to conventional cuprate $\text{La}_2\text{CuO}_{4-\delta}$, $\text{Ba}_2\text{CuO}_{4-\delta}$ displays compressed CuO_6 octahedra¹, which are inverted to the CuO_6 octahedra or CuO_5 pyramids in the parent phases and their derivatives of conventional cuprates La_2CuO_4 , $\text{YBa}_2\text{Cu}_3\text{O}_6$ ^{10,11}, etc.. This leads to unusual electronic states and superconducting nature⁵, in comparison with previous cuprates. Recently Scalapino *et al.* proposed that the active orbitals near the Fermi energy in $\text{Ba}_2\text{CuO}_{4-\delta}$ are $3d_{x^2-y^2}$ and $3d_{3z^2-y^2}$ ². Such a two-orbital character is distinctly different from the single band nature of conventional cuprates¹². Meanwhile, the effective single-band $t-J$ model was argued to be still applicable for the low-energy physics of the new cuprate^{3,4}. This debate immediately brings about the questions which scenario is applicable for superconducting $\text{Ba}_2\text{CuO}_{3.2}$, and which composition, Ba_2CuO_3 or the Ba_2CuO_4 , is the parent phase of superconducting $\text{Ba}_2\text{CuO}_{3.2}$.

Similar puzzle also may arise for earlier reported isostructural $\text{Sr}_2\text{CuO}_{4-\delta}$ with $T_c \approx 90\text{ K}^{13}$. Clarifying these questions is crucial for understand the superconducting nature of $\text{Ba}_2\text{CuO}_{3.2}$. On the other hand, it is well known that conventional cuprates, $\text{La}_2\text{CuO}_{4-\delta}$, $\text{YBa}_2\text{Cu}_3\text{O}_{7-\delta}$, etc., are strongly correlated systems with the Coulomb interaction considerably

larger than the kinetic bandwidth. The strong correlation of Cu 3d electrons not only leads to well localized magnetic moment of Cu spins, but also contributes non-Fermi liquid behavior and anomalous normal-state properties¹⁴. Presently it is not clear what role the electronic correlation plays in new superconductor in $\text{Ba}_2\text{CuO}_{4-\delta}$. Uncovering the roles of electronic correlations on the electronic states is also crucial for understanding the ground state and pairing mechanism in $\text{Ba}_2\text{CuO}_{4-\delta}$, as well as in $\text{Sr}_2\text{CuO}_{4-\delta}$. In the same time, considering the possible multiorbital character in $\text{Ba}_2\text{CuO}_{4-\delta}$ ², one may naturally question whether $\text{Ba}_2\text{CuO}_{4-\delta}$ is in the orbital selective Mott phase (OSMP) when the electron correlation is strong enough¹⁵.

Magnetic correlation has profound influences on the groundstate properties and magnetic structures of correlated systems. Previous works showed that spin correlations could considerably affect the magnetic groundstate and magnetic fluctuations of multiorbital Hubbard models¹⁶⁻²¹. It remains unknown in recent found $\text{Ba}_2\text{CuO}_{4-\delta}$, what the groundstate magnetic structures of two parent compounds Ba_2CuO_3 and $\text{Ba}_2\text{CuO}_{3.5}$ are? Clarifying these problems is important since as a new nonconventional superconductor, magnetic correlations and magnetic fluctuations are rather crucial for superconducting Cooper pairing.

In this work, we utilize the Kotliar-Ruckenstein slave boson technique to study the two-orbital Hubbard model of $\text{Ba}_2\text{CuO}_{4-\delta}$, focusing on the evolutions of the electronic states with the increasing filling number and electronic correlation, as well as the evolutions of the Fermi surfaces in the normal

state of in $\text{Ba}_2\text{CuO}_{4-\delta}$. In Sec. II, we first describe the Kotliar-Ruckenstein slave boson method. Then, in Sec. III, we discuss the numerical results. We find that when the electron concentration increases, the system evolves from a two-band character to a single-band ones when the doping concentration increases, as well as two distinct antiferromagnetic phases at electron filling of $n = 2$ and 3, respectively. To investigate the superconductivity in $\text{Ba}_2\text{CuO}_{4-\delta}$, in Sec. IV, we study the evolution of the pairing strength with the variations of the Coulomb correlation U and hole doping n within the random phase approximation. The discussions and conclusions are given in Sec. V.

II. MODEL HAMILTONIAN AND METHODS

We start from an effective two orbital Hubbard model at filling number $n = 1 + 2\delta$ for $\text{Ba}_2\text{CuO}_{4-\delta}^2$,

$$H = H_{kin} + H_{loc} \quad (1)$$

$$H_{kin} = \sum_{i,j,\alpha,\beta,\sigma} t_{ij}^{\alpha\beta} c_{i\alpha\sigma}^\dagger c_{j\beta\sigma} + \sum_{i,\alpha,\sigma} (\varepsilon_\alpha - \mu) n_{i\alpha\sigma} \quad (2)$$

$$H_{loc} = U \sum_{i,\alpha} n_{i\alpha\uparrow} n_{i\alpha\downarrow} + \sum_{i,\sigma,\sigma',\alpha>\beta} (U' - J_H \delta_{\sigma\sigma'}) n_{i\alpha\sigma} n_{i\beta\sigma'} - J_X \sum_{i,\alpha\neq\beta} c_{i\alpha\uparrow}^\dagger c_{i\alpha\downarrow} c_{i\beta\downarrow}^\dagger c_{i\beta\uparrow} + J_P \sum_{i,\alpha\neq\beta} c_{i\alpha\uparrow}^\dagger c_{i\alpha\downarrow}^\dagger c_{i\beta\downarrow} c_{i\beta\uparrow} \quad (3)$$

the $t_{ij}^{\alpha\beta}$ term describes electron hopping between the i -site with α orbital and the j -site with β orbital. $c_{i\alpha\sigma}^\dagger$ ($c_{j\beta\sigma}$) denotes the creation (annihilation) operator of an electron with spin $\sigma = \uparrow$ (\downarrow) and orbital α (β). $n_{i\alpha\sigma}$ is the corresponding occupation number operator. ε_α and μ are the energy level and chemical potential. In the interaction Hamiltonian term, H_{loc} , the intra-band and inter-band Coulomb repulsions are denoted by U and U' . J_H , J_X and J_P are the Hund's rule coupling divided into Ising term, spin-flip term and pair-hopping term, respectively. Here $J_X = J_P = 0$ that stands for Ising Hund's coupling case is adopted in this paper. Throughout this paper, we set $U' = U - 2J_H$ and $J_H = U/4$. To investigate the ground state magnetic properties of $\text{Ba}_2\text{CuO}_{4-\delta}$, we adopt the two-orbital tight-binding parameters given by T. Maier *et al* for the two e_g orbitals ($3d_{x^2-y^2}$, $3d_{3z^2-r^2}$) near the Fermi level². The orbital-dependent dispersions $T^{\alpha\beta}$ in the Hamiltonian are as follows²,

$$T^{11/22}(\mathbf{k}) = 2t_{x/y}^{11/22} (\cos k_x + \cos k_y) + 4t_{xy}^{11/22} \cos k_x \cos k_y + 2t_{xx/yy}^{11/22} (\cos 2k_x + \cos 2k_y), \quad (4)$$

$$T^{12/21}(\mathbf{k}) = 2t_{x/y}^{12/21} (\cos k_x - \cos k_y) + 2t_{xx/yy}^{12/21} (\cos 2k_x - \cos 2k_y) \quad (5)$$

The intra-orbital and inter-orbital hopping parameters are shown in Table I. The on-site energy of orbital $d_{x^2-y^2}$ is $\varepsilon_1 = -0.222$, and the on-site energy of orbital $d_{3z^2-r^2}$ is $\varepsilon_2 = \varepsilon_1 + \Delta$, where the crystal field splitting as a function of band filling n is given by $\Delta = 10.883 - 5n^2$.

TABLE I: The intra-orbital and inter-orbital hopping parameters of the two-orbital tight-binding model in eV^2 .

No.	1 st ($t_{x/y}$)	2 nd (t_{xy})	3 rd ($t_{xx/yy}$)
intra-orbital $d_{x^2-y^2}$	$t_{x/y}^{11} = -0.504$	$t_{xy}^{11} = 0.067$	$t_{xx/yy}^{11} = -0.13$
intra-orbital $d_{3z^2-r^2}$	$t_{x/y}^{22} = -0.196$	$t_{xy}^{22} = -0.026$	$t_{xx/yy}^{22} = -0.029$
inter-orbital	$t_{x/y}^{12} = 0.302$	$t_{xy}^{12} = 0$	$t_{xx/yy}^{12} = 0.051$

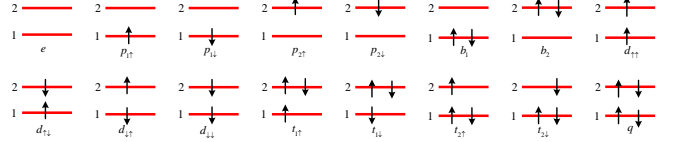


FIG. 1: (Color online) The atomic spin and orbital configurations of two-orbital system and the corresponding slave bosons. Here e , p , b , d , t , q denote empty, singly, and doubly occupied states in one orbital, doubly, triply and fully occupied states in different orbitals, respectively.

To investigate the magnetic groundstate properties of this model over wide electronic correlation, we use the Kotliar-Ruckenstein slave boson (KRSB) mean-field method²²⁻²⁴. In the KRSB framework, the local interaction term of the Hamiltonian can be projected by slave-boson operators, thus the interaction Hamiltonian term can be handled simply with saddle point approximation in the non-superconducting states. To describe the multi-orbital Hubbard model in KRSB representation, one should associate a boson creation operator ϕ_n^\dagger to every one of the 2^M Fock states, where M is the degree of each atom. The saddle-point value of the slave boson is interpreted as the probability of the corresponding Fock space configuration. For a two-orbital KRSB model, the sixteen Fock states in each site are shown in Fig.1 and the corresponding slave boson operators are also plotted. The sixteen slave bosons are classified into six categories according to the corresponding atomic configurations. We denote the slave boson operators ϕ_n^\dagger as $\{e^{(\dagger)}, p_{\alpha\sigma}^{(\dagger)}, d_{\sigma\alpha\sigma'}^{(\dagger)}, b_\alpha^{(\dagger)}, t_{\alpha\sigma}^{(\dagger)}, q^{(\dagger)}\}$. Here e is the slave boson for the empty state, $p_{\alpha\sigma}$ for the singly occupied state in orbital α with spin σ , $d_{\sigma\alpha\sigma'}$ for the doubly occupied state with a σ -spin electron in the α orbital and a σ' -spin electron in the β orbital. b_α for the doubly occupied state with a pair of up and down spin electrons in the α orbital. $t_{\alpha\sigma}$ for the triply occupied state with a pair of electrons in the β orbital and an extra σ -spin electron in the α orbital, q for the fully occupied state, respectively¹⁶.

With these slave boson operators, the realistic electronic states are described by these bosons and introduced auxiliary fermions $f_{\alpha\sigma}^\dagger$. Thus the realistic state $|n\rangle$ represented in the enlarged Hilbert space, which is the product of the slave bosons and the quasi-particle states, is as follows²⁵:

$$|n\rangle \equiv \phi_n^\dagger |Vac\rangle \otimes |n\rangle_f, \quad (6)$$

where the underline in $|n\rangle$ denotes the representative state in the enlarged Hilbert space and $|n\rangle_f$ is the n th Fock state in

the quasi-particle space. It is apparently not all the states in the enlarged Hilbert space have physical significance. To enforce the solution in the physical subspace in the enlarged Hilbert space, all the slave-boson operators should satisfy the following normalization constraint and the fermion number constraint:

$$\sum_{n=1}^{2^M} \phi_n^\dagger \phi_n = 1 \quad (7)$$

and

$$\hat{Q}_{\alpha\sigma}(\phi) = f_{\alpha\sigma}^\dagger f_{\alpha\sigma}, \quad \forall \alpha, \quad (8)$$

where

$$\hat{Q}_{\alpha\sigma}(\phi) \equiv \sum_{n=1}^{2^M} \langle n | f_{\alpha\sigma}^\dagger f_{\alpha\sigma} | n \rangle \phi_n^\dagger \phi_n. \quad (9)$$

In the KRSB framework, the Eq.(7) and Eq.(8) are rewritten as follows:

$$1 = e^\dagger e + \sum_{\alpha,\sigma} (p_{\alpha\sigma}^\dagger p_{\alpha\sigma} + t_{\alpha\sigma}^\dagger t_{\alpha\sigma}) + \sum_{\alpha} b_{\alpha}^\dagger b_{\alpha} + \sum_{\sigma,\sigma'} d_{\sigma\alpha\sigma'}^\dagger d_{\sigma\alpha\sigma'} + q^\dagger q, \quad (10)$$

$$f_{\alpha\sigma}^\dagger f_{\alpha\sigma} = p_{\alpha\sigma}^\dagger p_{\alpha\sigma} + b_{\alpha}^\dagger b_{\alpha} + \sum_{\sigma'} d_{\sigma\alpha\sigma'}^\dagger d_{\sigma\alpha\sigma'} + \sum_{\sigma'} t_{\beta\sigma'}^\dagger t_{\beta\sigma'} + t_{\alpha\sigma}^\dagger t_{\alpha\sigma} + q^\dagger q. \quad (11)$$

The electron creation operator should display the same character in the original Hilbert space and the enlarged Hilbert space, that is $\langle m | c_{\alpha\sigma}^\dagger | n \rangle = \langle m | c_{\alpha\sigma}^\dagger | n \rangle$, hence one has $\underline{c}_{\alpha\sigma}^\dagger = \sum_{mn} \langle n | c_{\alpha\sigma}^\dagger | m \rangle | n \rangle \langle m |$. According to Eq.(6), the electron creation operator in the enlarged Hilbert space is defined as $\underline{c}_{\alpha\sigma}^\dagger = \sum_{mn} \langle n | f_{\alpha\sigma}^\dagger | m \rangle \phi_n^\dagger \phi_m f_{\alpha\sigma}^\dagger$ ²⁵. To yield the noninteracting limit at saddle point approximation, a normalization term should be multiplied, thus the electron creation operator in the slave boson representation takes the form²⁵:

$$\underline{c}_{\alpha\sigma}^\dagger = f_{\alpha\sigma}^\dagger Z_{\alpha\sigma}^\dagger, \quad (12)$$

with

$$Z_{\alpha\sigma}^\dagger = \sum_{m,n=1}^{2^M} \hat{Q}_{\alpha\sigma}^{-\frac{1}{2}} \langle n | f_{\alpha\sigma}^\dagger | m \rangle \phi_n^\dagger \phi_m (1 - \hat{Q}_{\alpha\sigma})^{-\frac{1}{2}} \quad (13)$$

For a two-orbital system, the renormalization factor $Z_{\alpha\sigma}$ is given by¹⁶

$$Z_{\alpha\sigma} = \hat{Q}_{\alpha\sigma}^{-\frac{1}{2}} \left(p_{\alpha\sigma}^\dagger e + b_{\alpha}^\dagger p_{\alpha\sigma} + \sum_{\sigma'} d_{\sigma\alpha\sigma'}^\dagger p_{\beta\sigma'} + t_{\alpha\sigma}^\dagger b_{\beta} + \sum_{\sigma'} t_{\beta\sigma'}^\dagger d_{\sigma\alpha\sigma'} + q^\dagger t_{\alpha\sigma} \right) (1 - \hat{Q}_{\alpha\sigma})^{-\frac{1}{2}}, \quad (14)$$

The full Hamiltonian H can be expressed in terms of the slave-boson and quasi-particle fermionic variables. The expression of the projected Hamiltonian in the enlarged Hilbert space reads:

$$H = \sum_{\mathbf{k},\alpha,\beta,\sigma} T^{\alpha\beta}(\mathbf{k}) Z_{\alpha\sigma}^\dagger Z_{\beta,\sigma} f_{\mathbf{k}\alpha\sigma}^\dagger f_{\mathbf{k}\beta\sigma} + \sum_{\mathbf{k},\alpha,\sigma} (\varepsilon_{\alpha} - \mu) f_{\mathbf{k}\alpha\sigma}^\dagger f_{\mathbf{k}\alpha\sigma} + \sum_{n=1}^{2^M} \langle n | H_{loc} | n \rangle \phi_n^\dagger \phi_n. \quad (15)$$

Within saddle-point approximation we can obtain the groundstate energy of the system. The mean-field Hamiltonian with constraints can be diagonalized, and the variational total energy of the system is given by

$$E_{tot} = \sum_{\mathbf{k},n} E_n(\mathbf{k}) f(E_n(\mathbf{k})) + \sum_{n=1}^{2^M} \langle n | H_{loc} | n \rangle \phi_n^2 + \lambda \left(\sum_{n=1}^{2^M} \phi_n^2 - 1 \right) - \sum_{\alpha,\sigma} \eta_{\alpha\sigma} (Q_{\alpha\sigma} - n_{\alpha\sigma}), \quad (16)$$

where E_n is the eigenvalue of the Hamiltonian matrix and $f(E_n(\mathbf{k}))$ is the Fermi distribution function, λ and $\eta_{\alpha\sigma}$ are the Lagrange multipliers used to implement the constraints, Eq.(7) and Eq.(8), $n_{\alpha\sigma}$ is particle number of the orbital α with spin σ . The saddle-point equations are given by the partial derivatives of Eq.(16) to all of the slave-boson amplitudes and Lagrange multipliers. The self-consistent equations within saddle-point approximation are written as follows:

$$\frac{\partial E_{gs}}{\partial \phi_n} = \sum_{\mathbf{k},n,\alpha,\sigma} \frac{\partial E_n(\mathbf{k})}{\partial Z_{\alpha\sigma}} \frac{\partial Z_{\alpha\sigma}}{\partial \phi_n} + \sum_{n=1}^{2^M} 2 \langle n | H_{loc} | n \rangle \phi_n + \lambda \sum_{n=1}^{2^M} 2 \phi_n - \sum_{\alpha\sigma} \eta_{\alpha\sigma} \left(\frac{\partial Q_{\alpha\sigma}}{\partial \phi_n} - \frac{\partial n_{\alpha\sigma}}{\partial \phi_n} \right), \quad (17)$$

$$\frac{\partial E_{gs}}{\partial \lambda} = \sum_{n=1}^{2^M} \phi_n^2 - 1, \quad (18)$$

$$\frac{\partial E_{gs}}{\partial \eta_{\alpha\sigma}} = Q_{\alpha\sigma} - n_{\alpha\sigma} \quad (19)$$

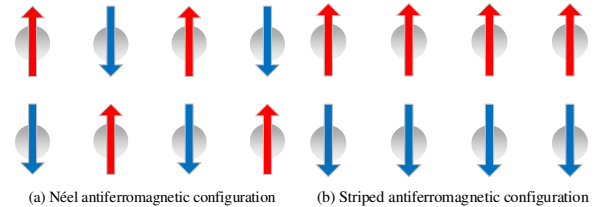


FIG. 2: (Color online) Two possible spin configurations of the Cu spins of (a) Néel AF, (b) Striped AF. The gray balls represent Cu atoms, the red and blue arrows denote the spin directions.

We get the ground state by solving the self-consistent equations through optimizing the objective function defined as¹⁷

$$F(\phi_n, \lambda, \eta_{\alpha\sigma}) = \sum_{n=1}^{2^M} \left(\frac{\partial E_{gs}}{\partial \phi_n} \right)^2 + \left(\frac{\partial E_{gs}}{\partial \lambda} \right)^2 + \sum_{\alpha\sigma} \left(\frac{\partial E_{gs}}{\partial \eta_{\alpha\sigma}} \right)^2. \quad (20)$$

Throughout this paper we compare the total energies of four possible candidates, paramagnetic metallic, ferromagnetic, Néel antiferromagnetic and striped antiferromagnetic phases, so as to find the most stable phase as the ground state. The latter two phases are shown in Fig.2.

To investigate the superconductivity in $\text{Ba}_2\text{CuO}_{4-\delta}$, based on the original Hamiltonian in Eqns.(1-5), we study the evolution of the pairing strength with the variations of the Coulomb correlation U and hole doping n through the random phase approximation. The pairing strength λ^α ($\alpha=s, d$ and g) could be obtained by solving the linearized gap equation²

$$-\sum_j \oint \frac{dk'_\parallel}{2\pi v_{Fj}(k'_\parallel)} \Gamma_{i,j}(k, k') g_j^\alpha(k') = \lambda_\alpha g_i^\alpha(k), \quad (21)$$

Here, α is the pairing channel, i and j are the band indices of Fermi surface vectors k, k' , respectively, $v_{Fj}(k'_\parallel)$ is the Fermi velocity, and $\Gamma_{i,j}(k, k')$ is the superconducting pairing interaction. With these equation we could well reproduce the results in Ref.[2].

III. NUMERICAL RESULTS

To demonstrate the effects of doping and electronic correlation on the electronic states, we present the numerical results of evolution of electronic states with the increasing U in the electron filling range of $2 < n < 3$. We find that the ferromagnetic state is always high energy, hence is neglected in what follows.

A. Paramagnetic Phases

We first present the evolutions of the band structures and the Fermi surfaces of paramagnetic $\text{Ba}_2\text{CuO}_{4-\delta}$ with increasing doping for $U=2$ and 4 eV, as shown in Fig.3 and Fig.4 respectively. We find that both for the intermediate correlation of $U=2$ eV and the strong correlation of $U=4$ eV, the systems are two bands near E_F for the filling number $n=2.1$ and 2.4 , and cross over to single band near E_F for the filling number $n=2.6$ and $n=2.9$, as in Fig.3. According to the analysis to the orbital weight of two-band situations and the single band situations, as seen the *supplementary material*, one finds that the two bands consist of the admixture of the $3d_{3z^2-r^2}$ and $3d_{x^2-y^2}$ orbitals due to considerable interorbital hopping t^{12} , and the single band mainly contributes from the $3d_{3z^2-r^2}$ orbital. For optimized doped superconducting phase $\text{Ba}_2\text{CuO}_{3.2}$, $n \approx 2.6$, only one correlation band crossing Fermi level suggests that $\text{Ba}_2\text{CuO}_{3.2}$ should be essentially a single band superconductor.

The doping evolution of the Fermi surfaces shown in Fig.4 further demonstrates the crossover character of two band scenario to single band one. Fig.4 shows that in the PM phase the electronic correlation does not change the Fermi surfaces too much, the doping drives the system crossover from two-type Fermi surfaces with electron and hole carriers to single hole Fermi surface, leading to the *Lifshitz* transition in $\text{Ba}_2\text{CuO}_{4-\delta}$.

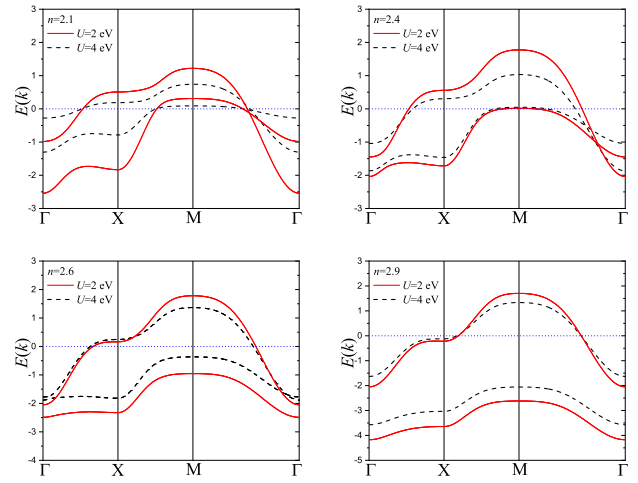


FIG. 3: (Color online) Dependence of the band structures on different doping in paramagnetic $\text{Ba}_2\text{CuO}_{4-\delta}$ at $U = 2$ (dotline) and $U = 4$ (dsahline).

The orbital weights of these Fermi surfaces are in agreement

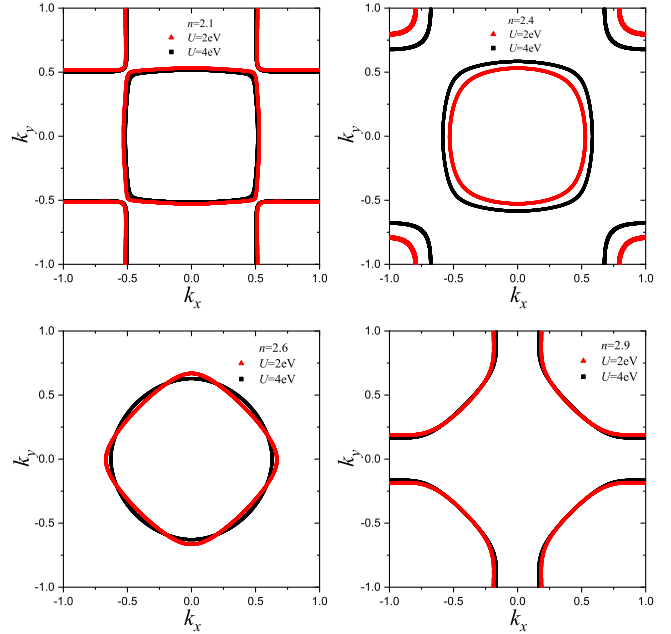


FIG. 4: (Color online) The Fermi surfaces of $\text{Ba}_2\text{CuO}_{4-\delta}$ for different doping at $U = 2$ and $U = 4$.

with those of the bands.

B. Magnetically Ordered Phases

In the presence of electronic correlation, the paramagnetic phase is usually unstable regarding to magnetically ordered phases. In this subsection we present the magnetic phase diagrams of $\text{Ba}_2\text{CuO}_{4-\delta}$ upon the increases of the electron cor-

relation U and the doping concentration. We first present two integer-filling compounds with $n=2$ and 3, which are two possible parent phases of superconducting states, and then the general doping case.

1. Half-filling Case

Firstly, we present the magnetic phase diagram of $\text{Ba}_2\text{CuO}_{4-\delta}$ on the correlation dependence at $n=2$ in Fig.5. This filling corresponds to one possible parent phase $\text{Ba}_2\text{CuO}_{3.5}$. The U -dependence of the total energies of the

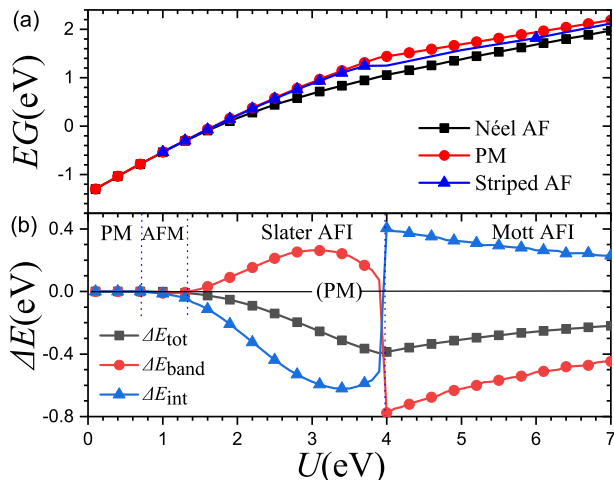


FIG. 5: (Color online) U dependence of the total energy E_{tot} of three different magnetic phases (a) and of the total, band and interaction energy differences ΔE_{tot} , ΔE_{band} and ΔE_{int} between the Néel AF and PM phases. Here PM, AFM and AFI denote the paramagnetic metallic phase, Néel antiferromagnetic metallic and insulating phases, respectively. Theoretical parameters: $n=2$, $J_H = U/4$

PM, the Néel AF and the striped AF states are shown in Fig.5(a). It shows that when $U < 0.65$ eV, these states are almost degenerate; when $U > 0.65$ eV, the total energy of the Néel AF state is considerably lower than the other two, suggesting that the Néel AF state is the most stable.

Analyzing the contributions of the kinetic or band energy and the potential or interaction energy to the total energy, we disclose the phase competition more detail, as shown in Fig.5(b). The total energy difference in Fig.5(b) is defined as $\Delta E_{\text{tot}} = E_{\text{Néel}} - E_{\text{PM}}$, and ΔE_{band} and ΔE_{int} denote the band and interaction energy differences between the Néel AF and PM phases, respectively. It can be seen that with the increasing electronic correlation, the system sequentially transits from the PM to the Néel AF metal, to the Slater AF insulator (AFI), and to the Mott AFI at $U_c=0.65, 1.3, 4$ eV, respectively. Here the Slater AFI phase is driven by interaction energy, so $\Delta E_{\text{int}} < 0$ and $\Delta E_{\text{band}} > 0$; on the contrast, the Mott AFI phase is driven by kinematic energy, so $\Delta E_{\text{int}} > 0$ and $\Delta E_{\text{band}} < 0$.²⁶ In the magnetically insulator the total energy difference between the PM and Néel AF states gives rise to the magnetic energy difference, or the spin coupling strength.

From Fig.5(b) one estimates that magnetic energy differences are about 100, 150, 230 and 400 meV for $U=2, 2.5, 3$ and 4 eV, respectively. These results demonstrate that when the system is in the intermediate correlation regime with $U = 2$ eV, the ground state is a Slater AFI; when it is in the strong correlation regime with $U > 4$ eV, the ground state is a Mott AFI.

2. Three-quarter filling case

Then we present the magnetic phase diagram of $\text{Ba}_2\text{CuO}_{4-\delta}$ on the correlation dependence at $n=3$, which is another possible parent phase of the superconducting state. The two-orbital model with the electron filling $n = 3$ describes the compound Ba_2CuO_3 . The U -dependences of the total energies in the PM, Néel AF, and striped AF configurations and of the energy differences are similar to Fig.5, except for the phase boundaries, as seen in Fig.6. One finds that when the electron correlation

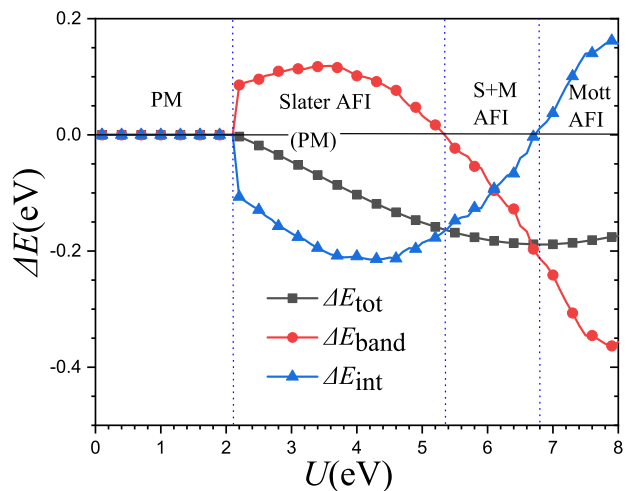


FIG. 6: (Color online) The U dependence of total energies of $\text{Ba}_2\text{CuO}_{4-\delta}$ in the PM, and Néel AF configurations (a) and of the energy differences ΔE_{tot} , ΔE_{band} , ΔE_{int} at $n=3$. Other parameters are the same to Fig.5.

increases from 0 to 8 eV, the sequentially quantum phase transitions from the PM to Slater AFI, and Slater AFI to Mott AFI happen at 2.1 and 6.8 eV, respectively. Comparing with the results at $n = 2$, we find that more large critical values U_c are needed to drive the PM-Slater AFI and the Slater-Mott AFI transitions. This demonstrate that when the system is in the intermediate correlation regime with $U < 2.1$ eV, the ground state is a PM; when it is in the strong correlation regime with $U > 4$ eV, the ground state is a Slater or Mott AFI. Meanwhile one notices that in Fig.6, the transition of the system from the PM to Slater AFI phases at $U = 2.1$ eV is the first order, this arises from the effect of the crystalline field splitting.

3. General Doping Cases

To explore the doping evolution and the electron correlation effect in $\text{Ba}_2\text{CuO}_{4-\delta}$, we obtain the general doping dependences of the magnetic phase diagrams, sublattice magnetic moments, and the Fermi surfaces at different correlation strengths of $U=2$ eV and 4 eV, respectively.

a. Magnetic Phase Diagrams After comparing the total energies of various magnetic configurations and determining the ground states for various doping, we plot the magnetic phase diagrams in the particle number range $2 < n < 3$ in Fig.7 at $U=2$ and 4 eV, respectively. Among various magnetic configurations, the PM, Néel and striped AF and ferromagnetic phase are taken into account. The ferromagnetic and striped AF phases are always unstable when $U < 4$, hence are neglected. So only the energy difference of the Néel AF state respect to the PM phase is plotted in Fig.7.

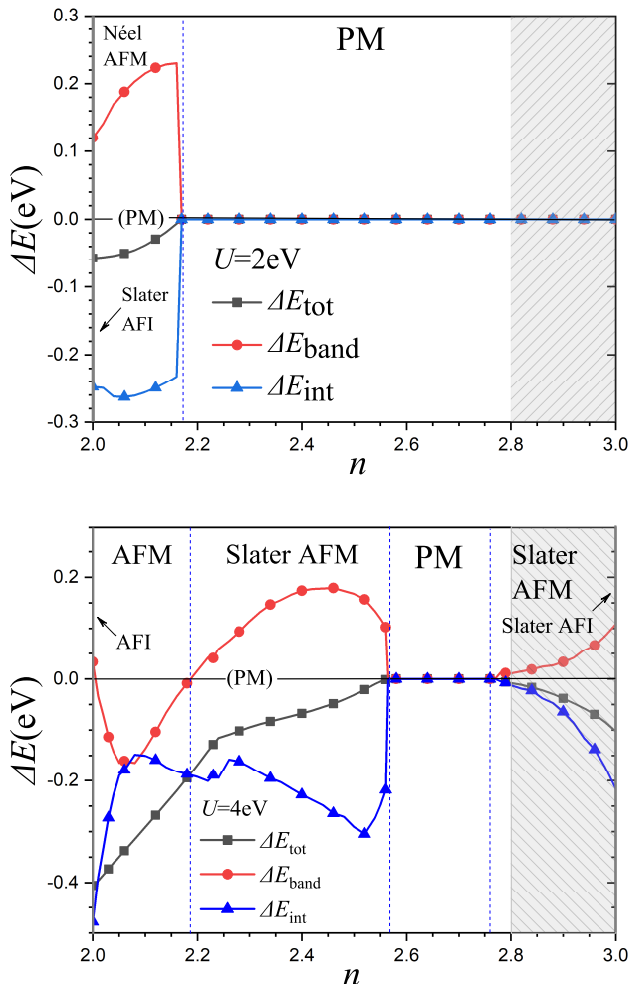


FIG. 7: (Color online) The magnetic phase diagrams of $\text{Ba}_2\text{CuO}_{4-\delta}$ and the energy differences between the PM state and the Néel AF state at $U=2$ eV (a) and $U=4$ eV (b).

One finds that in the intermediate correlation situation of

$U=2$ eV shown in Fig.7(a), the system is the Néel AF metallic (AFM) phase in the filling factor range of $2 < n < 2.18$; the system becomes the PM in the wide range of $2.18 < n < 3$. The dashed region denotes dominant single-band/orbital range. Such a simple magnetic phase diagram suggests that intermediate correlated $\text{Ba}_2\text{CuO}_{4-\delta}$ could not have two superconducting phases.

In the strongly correlated regime of $U=4$ eV shown in Fig.7(b), the magnetic phase diagram of the system is rich. With the increase of filling number n , the system first evolves from Mott AFI at $n=2$ to the Néel AFM phase in the filling factor range of $2 < n < 2.18$, where the energy gain ΔE_{int} and ΔE_{band} are both negative. This indicates that the AFM phase is interaction-energy and band-energy driven. With the further increasing n , only the energy gain ΔE_{int} are negative, the ground state of the system enters to Slater AFM phase due to the increasing Columb screening effect in the filling number range of $2.18 < n < 2.56$. Furthermore the system enters the PM state in $2.56 < n < 2.75$. One notices that the system transits from the AFM metallic to PM phase sharply at $n = 2.56$. This arises from the effect of the crystal field splitting, which leads to a first order transition. Further increasing n drives the system to another Slater AFM phase adjacent to the Slater AFI phase at $n=3$. In this range of $2.75 < n < 3.0$, the $d_{3z^2-r^2}$ orbital is closely fully occupied. The inter-orbital charge fluctuations and spin correlations are weak; thus the system becomes an effective single band model in the vicinity of three-quarter filling, as shown the shaded region in Fig.7(b), the energy gain of the AFM state is interaction-energy driven at $U = 4$.

b. Sublattice Magnetic Moments The evolution of electronic states of $\text{Ba}_2\text{CuO}_{4-\delta}$ is also reflected in the doping dependence of the sublattice magnetic moment of Cu spins at inequivalent sites. Fig.8 displays the evolution of the sublattice magnetic moment with increasing filling number n for different correlation strength of $U=2$ eV and 4 eV. In the intermediate correlation regime at $U=2$ eV, the magnetic moment, as seen the dashed line in Fig.8, is about $1.2 \mu_B$ in the AFM phase when $2 < n < 2.18$. In this region the active bands around Fermi level have two since $m > 1 \mu_B$. In strongly correlated $\text{Ba}_2\text{CuO}_{4-\delta}$ at $U = 4$ eV, as seen the solid line in Fig.8, the sublattice magnetic moment of Cu spins monotonically decreases from about $1.8 \mu_B$ at $n=2$ to about $0.7 \mu_B$ and diminishes to zero at $n=2.56$ in the first AFM region; Obviously, the compound in this region is a typical two-band system. In the second AFM region, the sublattice magnetic moment increases from zero to about $0.85 \mu_B$ when the filling number n increases from 2.68 to 3. This supports that the compound in this region is a single band system. Detail analysis shows that the active band is fully contributed by the electrons from the $d_{x^2-y^2}$ orbital.

c. Fermi Surfaces We also obtain the evolution of the Fermi surfaces of $\text{Ba}_2\text{CuO}_{4-\delta}$ with increasing filling number n at different correlation strengths. We plot the Fermi surfaces of the ground states of several typical filling numbers for $U=2$ eV in the upper panel and for $U=4$ eV in the lower panel of

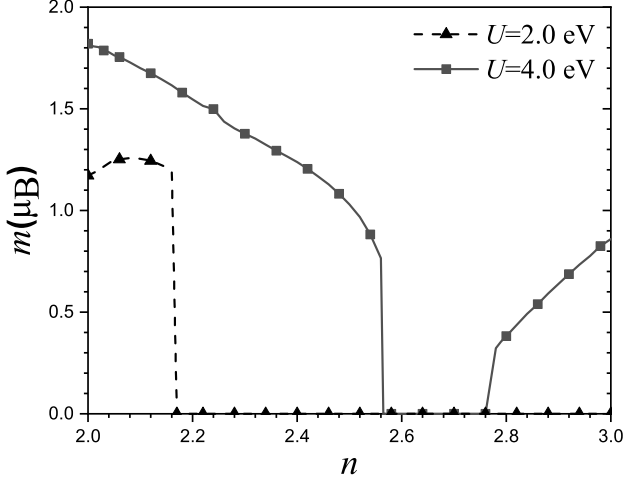


FIG. 8: (Color online) The sublattice magnetic moments of $\text{Ba}_2\text{CuO}_{4-\delta}$ at $U = 2$ eV (black line) and $U = 4$ eV (red line) as the functions of band filling .

Fig.9. The Brillouin zones with the dashlines indicate the folded zones due to the presence of the AF orders. From Fig.9 we find that in the intermediate correlation regime of $U=2$ eV, with the increase of filling number, the Fermi surfaces of the system evolve from 4 small hole pockets in the corners at $n=2.1$ to both 4 small hole Fermi surfaces in the corners and a large electron pocket in the zone center at $n=2.4$, then to a more large electron pocket in the zone center at $n=2.7$ since the hole pockets are fully filled. The presence of two kind Fermi surfaces is the direct consequence of two bands at $n=2.1$ and 2.4 .

In the strong correlation regime with $U=4$ eV, the evolution of the Fermi surfaces with increasing doping falls in expectation when $n < 2.7$. It is interested that at $n=2.9$, due to the strong correlation, a large electron Fermi surface splits into four separated small pockets in the centers of the zone edge .

IV. SUPERCONDUCTING PAIRING STRENGTH

To explore the unconventional superconductivity in $\text{Ba}_2\text{CuO}_{4-\delta}$, starting from the original two-orbital model Eqns.(1)-(5) we also perform the numerical calculations for the superconducting pairing strength arising from the spin-orbital fluctuations within the random phase approximation. We use the interaction parameters $U' = 0.5U$ and $J_H = J_P = U/4$ when calculating the pairing strength. The superconducting pairing strength of $\text{Ba}_2\text{CuO}_{3.2}$ as U increasing and the pairing strength of $\text{Ba}_2\text{CuO}_{4-\delta}$ as hole doping $2.35 < n < 2.65$ at $U = 2.0$ eV are presented in Fig.10.

We find that the dominant pairing symmetry is mixed s+d-wave or d-wave in the parameter ranges we are interested. It shows that at $n=2.6$, the pairing strength λ is negligible when the electronic correlation U is less than 1.6 eV; it becomes significantly with the s+d-wave pairing symmetry only when $U > 2$ eV and critically increases with the d-wave pairing

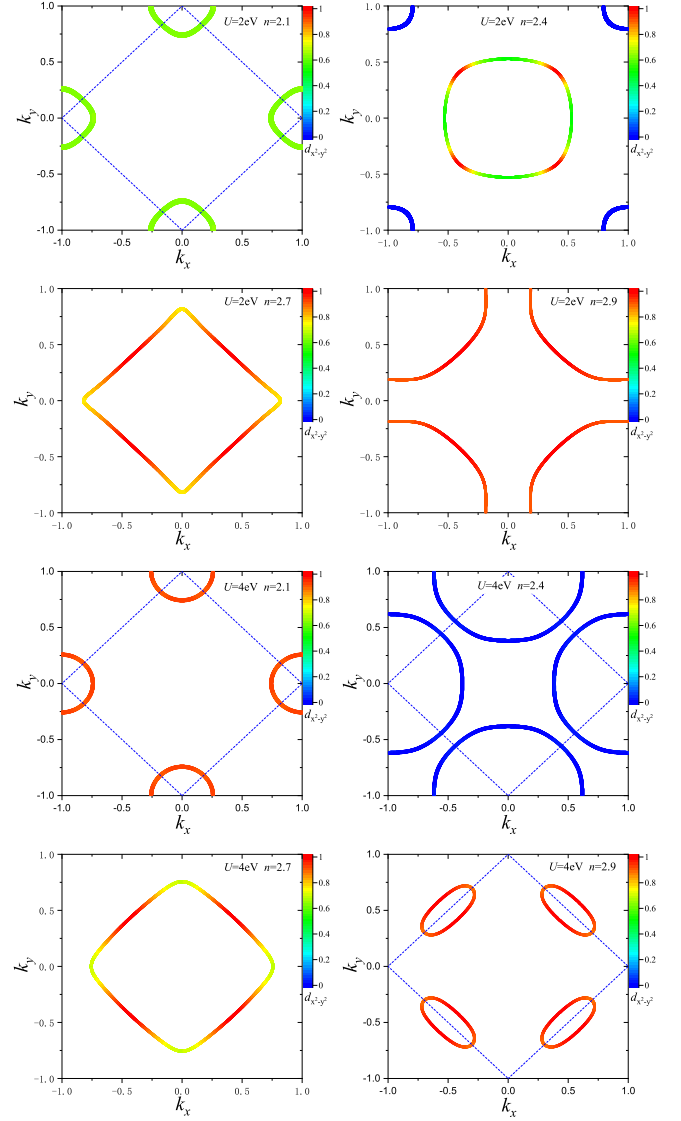


FIG. 9: (Color online) The evolutions of the Fermi surfaces of $\text{Ba}_2\text{CuO}_{4-\delta}$ with increasing doping at $U = 2$ (upper two panels) and $U = 4$ (lower two panels). The color represents the orbital weight of the $d_{x^2-y^2}$ (0) and $d_{3z^2-r^2}$ (1) orbitals .

symmetry when $U > 2.2$ eV, suggesting that superconducting $\text{Ba}_2\text{CuO}_{4-\delta}$ is at least in the intermediate or strong correlated regime. When $U > 2.4$ eV, the magnetic susceptibility and superconducting pairing strength diverge, more accurate methods, such as the fluctuation-exchange (FLEX) approximation, are expected. From the doping dependence of the pairing strength shown in the inset of Fig.10 we find that at $U=2$ eV, the λ does not monotonically vary with the electron filling number n . It shows that when $n < 2.38$ or $n > 2.61$, the pairing symmetry is d-wave dominant, and the s-wave symmetry becomes dominant when $2.38 < n < 2.61$. At the superconducting case $n=2.6$, the s-wave superconducting pairing strength becomes significant, meanwhile, the d-wave pairing weight can not be neglected, suggesting a possible s+d-wave

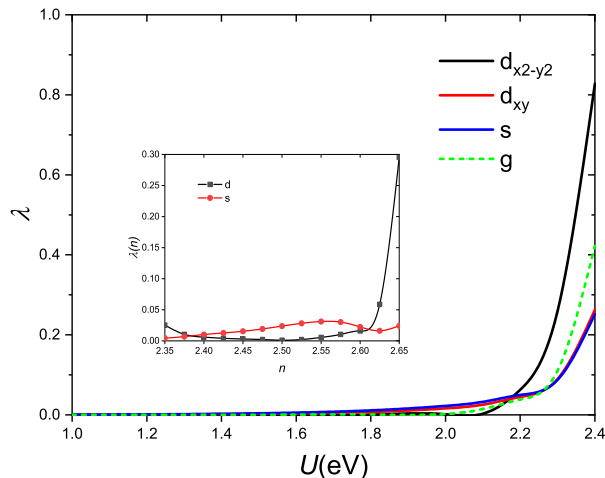


FIG. 10: (Color online) The evolutions of the superconducting pairing strength λ of $\text{Ba}_2\text{CuO}_{4-\delta}$ in the d-wave channel with the increasing correlations at $n=2.6$. Inset shows the dependence of the superconducting pairing strength λ on increasing doping at $U = 2$.

symmetry. These results demonstrate that the superconducting pairing strength of $\text{Ba}_2\text{CuO}_{3.2}$ is significantly finite.

V. DISCUSSIONS AND CONCLUSION

Therefore, regarding to the Scalapino *et al.*'s two active orbital model near the Fermi energy for recently discovered superconductor $\text{Ba}_2\text{CuO}_{4-\delta}$ with compressed octahedra, we have studied the influences of the electronic correlation, magnetic correlation and doping evolution on the groundstate properties of $\text{Ba}_2\text{CuO}_{4-\delta}$ by utilizing the Kotliar-Runkestein slave boson method. We demonstrate that at half filling, the correlated system displays two-band character with the orbital nature of $d_{3z^2-r^2}$ and $d_{x^2-y^2}$, and transits from the PM to AFM, the Slater AFI, and Mott AFI when the electronic correlation U continuously increases from weak to strong. It is worthy noting that $\text{Ba}_2\text{CuO}_{3.5}$ is the Slater AFI phase when $U > 1.3$ eV, or Mott AFI phase when $U > 4$ eV. At three-quarter filling, our study shows that the strongly correlated system exhibits single-band character with the orbital nature of $d_{x^2-y^2}$, and transits from the PM to the Slater AFI, S+M AFI, and Mott AFI when the electronic correlation increases from weak to strong. This Mott AFI phase is in agreement with the AF Mott insulator obtained by using the *GGA + U* method at large U for Ba_2CuO_3 . With the increasing doping concentration from 2 to 3, due to the crystalline field splitting effect, the system evolves from two-band character with the $d_{3z^2-r^2}$ and $d_{x^2-y^2}$ orbital nature to single-band one with the $d_{x^2-y^2}$ orbital nature both for intermediate and for strong correlations. Due to the magnetic correlation, when n varies from 2 to 3, the magnetic phase diagrams in the intermediate correlation regime and in the strong correlation regime are different: in

the former, there exists only one AF phase when $2 < n < 2.17$, in the latter the system displays first AF phase when $2 < n < 2.57$ and second AF phase when $2.76 < n < 3$. Notice that we here assume the oxygen vacancy is homogeneously distributed, do not consider partial or full oxygen order, which has been considered in a few recent works^{3,5}.

Regarding to concrete compound $\text{Ba}_2\text{CuO}_{3.2}$, from the preceding studies one notices that determining the electronic correlation strength U is crucial for understanding the properties of the normal and superconducting states of $\text{Ba}_2\text{CuO}_{3.2}$. This urges for more optical experiments, such as the X-ray absorption spectra (XAS) and resonant inelastic X-ray scattering, in high-quality $\text{Ba}_2\text{CuO}_{3.2}$ samples. Up to date, despite two XAS experiments by Li *et al.*¹ and Fumagalli *et al.*⁹ provided some information about the excited energy, a realistic U value remains unknown. Nevertheless, from the experimental spin coupling value about 150 meV⁹, comparing with the total-energy difference between the Neel AFM and paramagnetic phases shown in Fig.5, we estimate that $U \approx 2.5$ eV or so in $\text{Ba}_2\text{CuO}_{3.2}$, implying that $\text{Ba}_2\text{CuO}_{3.2}$ is at least an intermediate correlated system, or even a strongly correlated system. To exactly confirm the U value in $\text{Ba}_2\text{CuO}_{4-\delta}$ one needs to further perform the neutron scattering experiment to detect the magnetic moment per Cu spin and compare the theoretical magnetic moments in Fig.8.

Meanwhile, it is interested whether $\text{Ba}_2\text{CuO}_{4-\delta}$ could be a two-dome. when one takes $U=2 \sim 2.5$ eV for $\text{Ba}_2\text{CuO}_{4-\delta}$, our generalized magnetic phase diagrams in Fig.7, as well as the doping evolutions of the band structures in Fig.3 and of the Fermi surfaces in Fig.9, show that $\text{Ba}_2\text{CuO}_{3.2}$ is essentially a single-band superconductor, though this band consists of hybridized $d_{x^2-y^2}$ and $d_{3z^2-r^2}$ orbitals. In this correlation regime, the system behaves as single-band paramagnetic when $n > 2.2$, or $\delta > 0.6$, and has only one AFM parent phase, thus precludes the two-dome superconducting phases. Only in the strongly correlated regime with $U > 4$ eV, can the system display two different AFM parent phases at $n=2$ and 3, corresponding to two-band and single-band nature, respectively. In this situation, different type spin fluctuations contribute different superconducting pairing strengths, suggesting the possibility of two-dome superconducting phases. A few of recent theoretical works suggested $\text{Ba}_2\text{CuO}_{4-\delta}$ is weak correlated², or strong correlated^{3,5}; we expect further experiment could finally resolve this issue.

Acknowledgments

This work was supported by the National Natural Science Foundation of China under Grant nos. 11774350 and 11534010, The calculations were performed in Center for Computational Science of CASHIPS, and partly using Tianhe-2JK computing time award at the Beijing Computational Science Research Center(CSRC).

-
- * These authors contributed equally.
[†] zou@theory.issp.ac.cn
- ¹ W. M. Li, J. F. Zhao, L. P. Cao, Z. Hu, Q. Z. Huang, X. C. Wang, Y. Liu, G. Q. Zhao, J. Zhang, Q. Q. Liu, et al., *Proc. Natl. Acad. Sci. USA* **116**, 12156 (2019).
 - ² T. Maier, T. Berlijn, and D. J. Scalapino, *Phys. Rev. B* **99**, 224515 (2019).
 - ³ K. Liu, Z. Y. Lu, and T. Xiang, *Phys. Rev. Mater.* **3**, 044802 (2019).
 - ⁴ Z. Wang, S. Zhou, W. Q. Chen, and F. C. Zhang, *Phys. Rev. B* **101**, 180509 (2020).
 - ⁵ K. Jiang, C. Le, Y. Li, S. Qin, Z. Wang, F. Zhang, and J. Hu, *Phys. Rev. B* **103**, 045108 (2021).
 - ⁶ Y. H. Li, S. Q. Du, Z. Y. Weng, and Z. Liu, *Phys. Rev. Mater.* **4**, 044801 (2020).
 - ⁷ K. Yamazaki, M. Ochi, D. Ogura, K. Kuroki, H. Eisaki, S. Uchida, and H. Aoki, *Phys. Rev. Res.* **2**, 033356 (2020).
 - ⁸ A. M. Oles, K. Wohlfeld, and G. Khaliullin, *Condens. Matter* **4** (2019).
 - ⁹ R. Fumagalli, A. Nag, S. Agrestini, M. Garcia-Fernandez, A. C. Walters, D. Betto, N. B. Brookes, L. Braicovich, K.-J. Zhou, G. Ghiringhelli, et al., *Physica C: Superconductivity and its Applications* **581**, 1353810 (2021).
 - ¹⁰ B. Grande, H. Muller-Buschbaum, and M. Schweizer, *Z. Anorg. Allg. Chem.* **428**, 120 (1977).
 - ¹¹ J. S. Swinnea and H. Steinink, *J. Mater. Res.* **2**, 424 (1987).
 - ¹² F. C. Zhang and T. M. Rice, *Phys. Rev. B* **37**, 3759 (1988).
 - ¹³ S. D. Conradson, T. H. Geballe, C. Jin, L. Cao, A. Gauzzi, M. Karppinen, G. Baldinozzi, W. Li, E. Gilioli, J. M. Jiang, et al., *Proc. Natl. Acad. Sci. USA* **117**, 33099 (2020).
 - ¹⁴ P. A. Lee, N. Nagaosa, and X. G. Wen, *Rev. Mod. Phys.* **78**, 17 (2006).
 - ¹⁵ Y. Ni, Y.-M. Quan, J. Liu, Y. Song, and L.-J. Zou, *Phys. Rev. B* **103**, 214510 (2021).
 - ¹⁶ Y. M. Quan, L. J. Zou, D. Y. Liu, and H. Q. Lin, *Eur. Phys. J. B* **85**, 55 (2012).
 - ¹⁷ Y. M. Quan, Q. W. Wang, D. Y. Liu, X. L. Yu, and L. J. Zou, *Comput. Phys. Commun.* **191**, 90 (2015).
 - ¹⁸ Y. M. Quan, D. Y. Liu, and L. J. Zou, *Acta Phys. Sin.* **61**, 017106 (2012), [in Chinese].
 - ¹⁹ Y. M. Quan, D. Y. Liu, H. Q. Lin, and L. J. Zou, *J. Magn. Magn. Mater.* **456**, 329 (2018).
 - ²⁰ H. Lee, Y. Z. Zhang, H. O. Jeschke, and R. Valentí, *Phys. Rev. B* **84**, 020401 (2011).
 - ²¹ Y. Z. Zhang, H. Lee, H. Q. Lin, C. Q. Wu, H. O. Jeschke, and R. Valentí, *Phys. Rev. B* **85**, 035123 (2012).
 - ²² G. Kotliar and A. E. Ruckenstein, *Phys. Rev. Lett.* **57**, 1362 (1986).
 - ²³ A. Ruegg, M. Indergand, M. Indergand, and M. Sigrist, *Eur. Phys. J. B* **48**, 55 (2005).
 - ²⁴ H. Hasegawa, *Phys. Rev. B* **56**, 1196 (1997).
 - ²⁵ F. Lechermann, A. Georges, G. Kotliar, and O. Parcollet, *Phys. Rev. B* **76**, 155102 (2007).
 - ²⁶ H. Watanabe, T. Shirakawa, and S. Yunoki, *Phys. Rev. B* **89**, 165115 (2014).